Uncovering Early Galaxy Evolution in the ALMA and JWST Era
Proceedings IAU Symposium No. 352, 2019
E. da Cunha, J. Hodge, J. Afonso, L. Pentericci & D. Sobral, eds.

doi:10.1017/S1743921319008974

Automated mining of the ALMA archive in the COSMOS field (A^{3}COSMOS): Cold molecular gas evolution

Daizhong Liu[1] and A^{3}COSMOS Team[2]

[1]Max-Planck-Institut für Astronomie,
Königstuhl 17, D-69117 Heidelberg, Germany
email: dzliu@mpia.de

[2]https://sites.google.com/view/a3cosmos/team

Abstract. We present new constraints on the cosmic cold molecular gas evolution out to redshift 6 based on systematic mining of the public ALMA archive in the COSMOS field (A^{3}COSMOS). Our A^{3}COSMOS dataset contains ∼700 galaxies ($0.3 \lesssim z \lesssim 6$) with high-confidence ALMA detection and multi-wavelength SEDs. Combining with ∼1,200 CO-observed galaxies at $0 \lesssim z \lesssim 4$ (75% at $z < 0.1$) in the literature, we parameterize galaxies' molecular gas depletion time and gas fraction each as a function of stellar mass, offset from the star-forming main-sequence and cosmic age. We propose a new functional form which provides a better fit and implies a "downsizing" effect and "mass-quenching". By adopting galaxy stellar mass functions and applying our gas fraction function, we obtain a cosmic cold molecular gas density evolution in agreement with recent CO blind field surveys as well as semi-analytic modeling. These together provide us a coherent picture of galaxy cold molecular gas, SFR and stellar mass evolution.

Keywords. galaxies: evolution — galaxies: high-redshift — galaxies: ISM — submillimeter

1. Introduction

Cold molecular gas is the fuel of star formation activity in galaxies. In recent years, our knowledge of the cosmic evolution of star formation and stellar mass growth has been obtained out to redshift ∼5, however, the cosmic evolution of the cold molecular gas is much less well constrained, and the validity of different methods are debated.

Briefly, there are three most widely used methods for probing gas mass in high-redshift galaxies: *(1)* blind deep field CO luminosity function and CO-to-H_2 conversion method (e.g., Walter *et al.* 2014; Decarli *et al.* 2016, 2019; Riechers *et al.* 2019); *(2)* IR-to-millimeter(mm) spectral energy distribution (SED) fitting dust mass to gas mass method (e.g., Santini *et al.* 2010, 2014; Magdis *et al.* 2011, 2012; Magnelli *et al.* 2012, 2014; Genzel *et al.* 2015); and *(3)* Rayleigh-Jeans(RJ)-tail dust continuum to gas mass calibration method (e.g., Scoville *et al.* 2014, 2016, 2017; Groves *et al.* 2015; Schinnerer *et al.* 2016; Hughes *et al.* 2017).

Earlier works have led to a coevolution picture of dust, gas and star formation from redshift 3 to present where: *(a)* the molecular gas to total baryon mass fraction, $f_{\rm mol\,gas} \equiv M_{\rm mol\,gas}/(M_{\rm mol\,gas} + M_\star)$, or $\mu_{\rm molgas} \equiv M_{\rm mol\,gas}/M_\star$, increases with redshift and depends slightly on the SFR and stellar mass; *(b)* the molecular gas depletion time, $\tau_{\rm depl} \equiv M_{\rm mol\,gas}/{\rm SFR}$, decreases with redshift and also depends on SFR and stellar mass; *(c)* whereas $\tau_{\rm depl}$ and $\mu_{\rm molgas}$ more primely correlated with the $M_\star - {\rm SFR}$ main-sequence (MS; e.g., Speagle *et al.* 2014), denoted as $\delta{\rm MS} \equiv {\rm SFR}/{\rm SFR}_{\rm MS}$, or $\Delta{\rm MS} \equiv \log_{10}({\rm SFR}/{\rm SFR}_{\rm MS})$, than the absolute SFR or specific-SFR ($\equiv {\rm SFR}/M_\star$).

While the aforementioned trends have been widely studied at local and high redshift, an accurate parametrization ($\mu_{\rm molgas}$ and $\tau_{\rm depl}$ functions) across the parameter space is still under debate. Utilizing the RJ-tail dust continuum method (at rest-frame 850 μm), Scoville *et al.* (2017, hereafter S17) studied a sample of 708 high-redshift *Herschel*-selected galaxies ($0.3 < z < 4.5$) which have detection with Atacama Large Millimeter/submillimeter Array (ALMA), and characterized the $\mu_{\rm molgas}$ and $\tau_{\rm depl}$ functions as:

$$\mu_{\rm molgas} = 0.71 \times (\delta{\rm MS})^{+0.32} \times M_{\star,10}^{-0.70} \times (1+z)^{+1.84},$$
$$\tau_{\rm depl} = 3.23\ {\rm Gyr} \times (\delta{\rm MS})^{-0.70} \times M_{\star,10}^{-0.01} \times (1+z)^{-1.04}, \quad (1.1)$$

where $M_{\star,10} \equiv M_\star/(10^{10}\ {\rm M}_\odot)$. With the same method but at rest-frame 250–500 μm, Schinnerer *et al.* (2016) studied a smaller, optically-selected sample at $z = 2.8 - 3.6$. However, discrepancies exist due to the different wavelengths and samples. Tacconi *et al.* (2018, hereafter T18) expanded the work of Genzel *et al.* (2015) using all three methods to obtain the molecular gas masses for 1,444 galaxies at $0 < z < 4$ (including stacking), and fitted them all together to derive the $\mu_{\rm molgas}$ and $\tau_{\rm depl}$ functions:

$$\mu_{\rm molgas} = 0.75 \times (\delta{\rm MS})^{+0.53} \times M_{\star,10}^{-0.35} \times 10^{-3.62\times(\log_{10}(1+z)-0.66)^2},$$
$$\tau_{\rm depl} = 1.06\ {\rm Gyr} \times (\delta{\rm MS})^{-0.44} \times M_{\star,10}^{+0.09} \times (1+z)^{-0.62}, \quad (1.2)$$

where we adapted their equation to $M_{\star,10}$ (same as in Eq. 1.1) and ignored galaxy size dependency. Comparing Eqs. 1.1 and 1.2 at redshift 3 and $M_\star = 5 \times 10^{10}\ {\rm M}_\odot$ reveals a factor of 6 difference in $\mu_{\rm molgas}$ and a factor of 1.5 in $\tau_{\rm depl}$. Such noticeable differences exist for other parameter values as well, raising concerns on the validity and predictability of the $\mu_{\rm molgas}$ and $\tau_{\rm depl}$ functions. In addition, previous works have constraints only for $z \lesssim 3$.

To solve the discrepancies and understand systematic biases, a large, robust galaxy sample from local to high redshift is needed to carry out the comprehensive analysis. Therefore, here we briefly present our A^{3}COSMOS gas evolution study, where we: *(a)* developed automated pipelines for public ALMA archive data reduction, imaging, photometry, statistical corrections and extensive analyses (see Liu *et al.* 2019 ApJS in press; hereafter paper I), *(b)* combined with 1,200+ CO-detected galaxies at $0 \lesssim z \lesssim 4$ (75% at $z < 0.1$) in the literature to build a largest, most robust sample ($\sim 2,000$), *(c)* obtained new parameterization of $\mu_{\rm molgas}$ and $\tau_{\rm depl}$ by fitting the new data, and *(d)* applied galaxy stellar mass functions and/or galaxy modelings to obtain the final cosmic molecular gas mass density evolution. The full content of this work is presented in Liu *et al.* (to be submitted; hereafter paper II). Here we only highlight the main results.

2. Method

We developed automated pipelines to query and reduce ALMA public archival data (in the COSMOS 2 sq. deg. field), and pipelines for blind-extraction and prior-based photometry, Monte Carlo simulations and photometry quality assessments. This results into nearly 1,900 ALMA imaging products, 1,200+ robust ALMA detections (version 20180801). Fig. 1 shows the spatial distribution of all these ALMA images (we used all ALMA bands). We select the robust ALMA detections with a relatively high signal-to-noise ratio which correspond to about 10% spurious fraction according to our statistical analysis. Then we performed various quality assessment steps to identify most plausible spurious sources (e.g., boosted by noise or blended with other sources) and excluded them from our final robust galaxy catalog (about 700 galaxies with multi-wavelength SEDs, some have multiple-ALMA-band detections).

https://doi.org/10.1017/S1743921319008974 Published online by Cambridge University Press

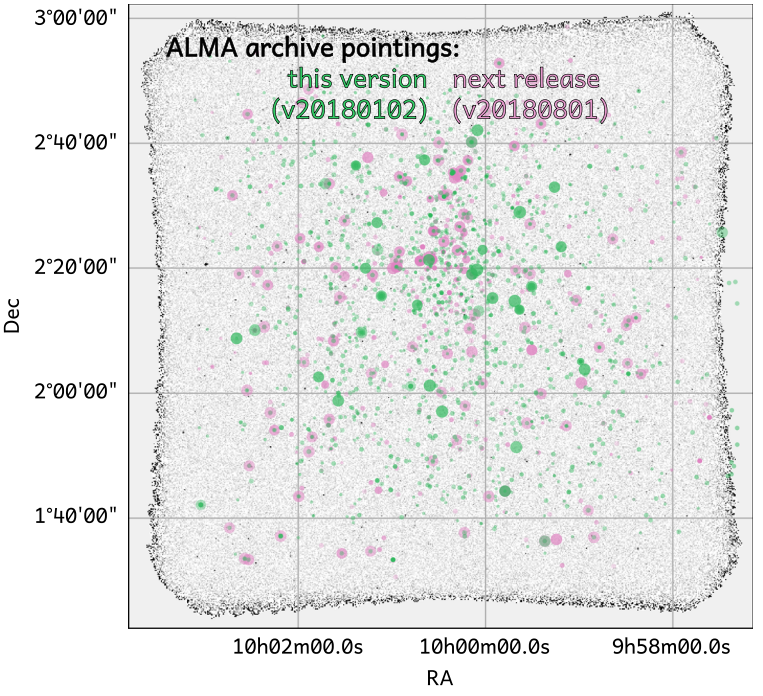

Figure 1. ALMA pointings in the COSMOS field that are publicly accessible. Green and magenta circles represent ALMA pointings which became public before Jan. 2nd, 2018 and Aug. 1st, 2018 respectively. Circle sizes represent the FWHM of the ALMA 12m antennas' primary beam, and the shading reflects the on-source integration time (dark referring to longer integration times). The background image is the *Herschel* PACS 100 μm data from the PACS Evolutionary Probe survey (PEP; Lutz *et al.* 2011).

We included 16 samples of galaxies with CO observations in the literature as complimentary information to our analysis. The full list is presented in our paper II. It encompasses most of the CO-observed samples analyzed by T18. Most of these samples are galaxies in the local Universe, and the largest sample is from the xCOLD GASS survey (Saintonge *et al.* 2017).

In our paper II, we also compared various dust-based gas mass calculation methods, i.e., MAGPHYS (da Cunha *et al.* 2008) SED-fitted dust mass method, RJ 850μm (Scoville *et al.* 2014, 2016, Hughes *et al.* 2017); and RJ 250–500μm method (Groves *et al.* 2015).

We analyzed the complicated dependencies of $\tau_{\rm depl}$ and $\mu_{\rm molgas}$ (respectively) on galaxies' redshift, stellar mass and ΔMS properties. Motivated by the high-dimensional data fitting, we propose a new functional form which accounts for the different behaviors of galaxies due to their stellar masses:

$$\begin{aligned}\log_{10}\tau_{\rm depl} &= (\mathsf{a}+\mathsf{ak}\times\log_{10}(M_\star/10^{10}))\times\Delta{\rm MS}+\mathsf{b}\times\log_{10}(M_\star/10^{10})\\ &\quad+(\mathsf{c}+\mathsf{ck}\times\log_{10}(M_\star/10^{10}))\times t_{\rm cosmic\ age}+\mathsf{d}\\ \log_{10}\mu_{\rm molgas} &= (\mathsf{a}+\mathsf{ak}\times\log_{10}(M_\star/10^{10}))\times\Delta{\rm MS}+\mathsf{b}\times\log_{10}(M_\star/10^{10})\\ &\quad+(\mathsf{c}+\mathsf{ck}\times\log_{10}(M_\star/10^{10}))\times t_{\rm cosmic\ age}+\mathsf{d}\end{aligned}\quad(2.1)$$

The coefficients a, b, c, d, ak and ck for either $\tau_{\rm depl}$ and $\mu_{\rm molgas}$ (respectively) are provided in our paper II. In Fig. 2 we present the data, fitted functions in this work and from T18 and S17. The parameterizations of $\tau_{\rm depl}$ and $\mu_{\rm molgas}$ with our, T18 and S17 functions are roughly consistent within the overlapping regions of the parameter space, i.e., $z\sim1-3$,

https://doi.org/10.1017/S1743921319008974 Published online by Cambridge University Press

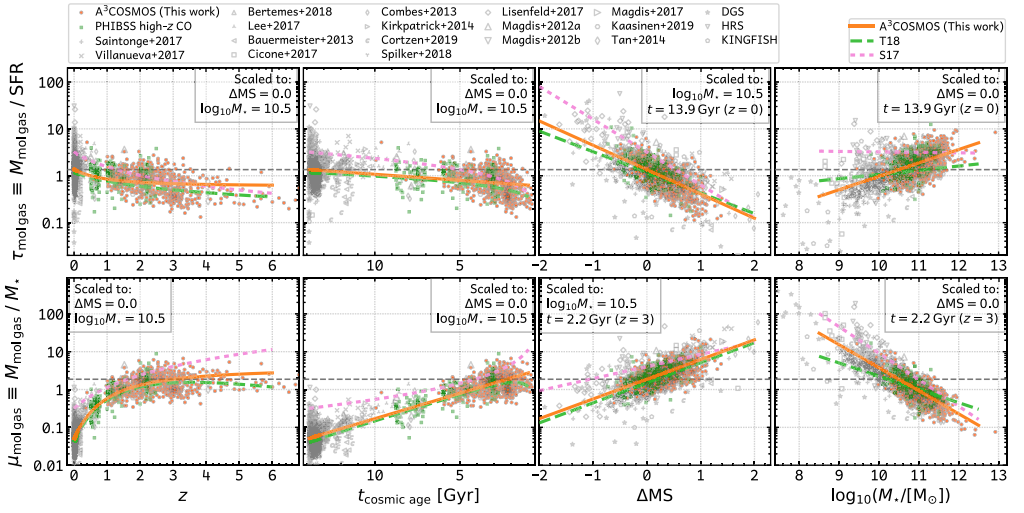

Figure 2. Characterizing molecular gas depletion time $\tau_{\rm depl}$ (*upper panels*) and molecular gas to stellar mass ratio $\mu_{\rm molgas}$ (*lower panels*) in the functional form of Eq. 2.1. From *left* to *right*, we show $\tau_{\rm depl}$ versus redshift, $t_{\rm cosmic\,age}$, ΔMS and $M_\star$, respectively. Data points in each panel are re-scaled using the best-fit function so as to remove the dependency on other parameters and leave only the correlation with the current X-axis parameter (with coefficient(s) labeled at the bottom of each panel). Orangered data points are from this work, while green ones are from PHIBSS 1&2 surveys (T18) and gray ones are from the literature as listed at the top. Our best-fit function is shown as the solid orangered line in each panel, while the functions from T18 (Eq. 1.2) and S17 (Eq. 1.1) are shown as the dashed green and dotted gray lines, respectively.

$\Delta{\rm MS} > 0$ and $\log M_\star > 10.5$. They differ significantly for low-mass and/or main-sequence or below-main-sequence galaxies, which however cannot be verified with current dataset.

Our function implies a "downsizing" effect, i.e., more-massive galaxies evolve earlier than less-massive ones, and "mass-quenching", i.e., gas depletion slows down with cosmic time for more-massive galaxies but speeds up for less-massive ones (see our paper II).

3. Results

The $\mu_{\rm molgas}$ function allows us to infer a galaxy's molecular gas mass with its known z, SFR and $M_\star$. Although this is very uncertain for an individual galaxy, it statistically works for large samples of galaxies. Therefore, if we know galaxy populations and their number densities, e.g., stellar mass functions (SMFs), then by integrating all star-forming galaxies at each redshift we are able to obtain the cosmic molecular gas mass density.

For the first time we provide such an estimation (from gas fraction scaling relations) as detailed in our paper II. Fig. 3 shows three cosmic molecular gas density evolution curves by applying our, T18 and S17 $\mu_{\rm molgas}$ functions, respectively, to the SIDES mock galaxy modeling of Béthermin *et al.* (2017) who fully simulated galaxies within a 2 sq. deg. COSMOS-like field with best-known SMFs, galaxy number counts, infrared/sub-mm luminosity functions and clustering. The differences are mainly driven by the extrapolation of these functions to the lower-mass/below-MS and/or $z > 3$ galaxies. CO blind deep field results from Decarli *et al.* (2016, 2019) and Riechers *et al.* (2019), and semi-analytic modeling from Popping *et al.* (2019) are shown for comparison.

This strongly supports that we now have a coherent picture of galaxies' star formation, stellar mass and molecular gas evolution, which can be well-parameterized by the main sequence correlation (e.g., Speagle *et al.* 2014 #49 with cosmic time), stellar mass

https://doi.org/10.1017/S1743921319008974 Published online by Cambridge University Press

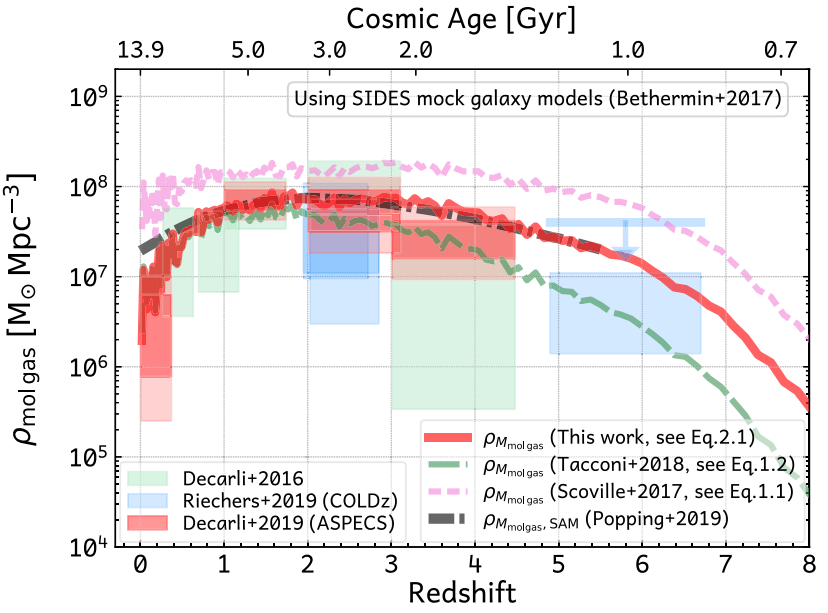

Figure 3. Cosmic evolution of cold molecular gas mass density. Results from high-z CO blind deep field studies from Decarli *et al.* (2016), Riechers *et al.* (2019) and Decarli *et al.* (2019) are shown as green, blue and red boxes, with the X-sides (Y-sides) indicating the observed redshift range ($5^{\rm th}$ and $95^{\rm th}$ percentiles) (the $z\sim6$ arrow is an upper limit from Riechers *et al.* 2019). The red solid, green long-dashed and purple short-dashed lines are the integrated molecular gas mass density based on the mock galaxy modeling by Béthermin *et al.* (2017) (integrated down to $M_\star = 10^{9.0}\,{\rm M}_\odot$) and gas fraction function from this work (Eq. 2.1), T18 and S17, respectively. The black dash-dot line is from the Semi-Analytic Model (SAM) simulation of Popping *et al.* (2019). More details in our paper II.

functions (e.g., see references in Béthermin *et al.* 2017) and gas scaling relations (e.g., with our new functional form in Eq. 2.1), respectively.

References

Béthermin, M., *et al.* 2017, *A&A*, 607, A89
da Cunha, E., Charlot, S., & Elbaz, D. 2008, *MNRAS*, 388, 1595
Decarli, R., *et al.* 2016, *ApJ*, 833, 69
—. 2019, arXiv e-prints, arXiv:1903.09164
Genzel, R., *et al.* 2015, *ApJ*, 800, 20
Groves, B. A., *et al.* 2015, *ApJ*, 799, 96
Hughes, T. M., *et al.* 2017, *MNRAS*, 468, L103
Liu, *et al.* 2019, *ApJS*, 244, 42
Lutz, D., *et al.* 2011, *A&A*, 532, A90
Magdis, G. E., *et al.* 2011, *ApJL*, 740, L15
—. 2012, *ApJ*, 760, 6
Magnelli, B., *et al.* 2012, *A&A*, 548, A22
—. 2014, *A&A*, 561, A86
Popping, G., *et al.* 2019, arXiv e-prints, arXiv:1903.09158
Riechers, D. A., *et al.* 2019, *ApJ*, 872, 7
Saintonge, A., *et al.* 2017, *ApJS*, 233, 22
Santini, P., *et al.* 2010, *A&A*, 518, L154
—. 2014, *A&A*, 562, A30
Schinnerer, E., *et al.* 2016, *ApJ*, 833, 112

https://doi.org/10.1017/S1743921319008974 Published online by Cambridge University Press

Scoville, N., *et al.* 2014, *ApJ*, 783, 84
—. 2016, *ApJ*, 820, 83
—. 2017, *ApJ*, 837, 150
Speagle, J. S., *et al.* 2014, *ApJS*, 214, 15
Tacconi, L. J., *et al.* 2018, *ApJ*, 853, 179
Walter, F., *et al.* 2014, *ApJ*, 782, 79

https://doi.org/10.1017/S1743921319008974 Published online by Cambridge University Press